nature physics

LETTERS

PUBLISHED ONLINE: 22 SEPTEMBER 2013 | DOI: 10.1038/NPHYS2762

A large-energy-gap oxide topological insulator based on the superconductor $BaBiO_3$

Binghai Yan[1,2,3]*, Martin Jansen[1] and Claudia Felser[1,3]

Topological insulators are a new class of quantum materials that are characterized by robust topological surface states (TSSs) inside the bulk insulating gap[1,2], which hold great potential for applications in quantum information and spintronics as well as thermoelectrics. One major obstacle is the relatively small size of the bulk bandgap, which is typically around 0.3 eV for the known topological insulator materials (ref. 3 and references therein). Here we demonstrate through *ab initio* calculations that a known superconductor $BaBiO_3$ (BBO) with a T_c of nearly 30 K (refs 4,5) emerges as a topological insulator in the electron-doped region. BBO exhibits a large topological energy gap of 0.7 eV, inside which a Dirac type of TSSs exists. As the first oxide topological insulator, BBO is naturally stable against surface oxidization and degradation, distinct from chalcogenide topological insulators[6–8]. An extra advantage of BBO lies in its ability to serve as an interface between TSSs and superconductors to realize Majorana fermions for future applications in quantum computation[9].

Mixed-valent perovskite oxides based on BBO (refs 4,5) are, like cuprates, well-known superconductors. The parent compound BBO crystallizes in a mononclinic lattice[10] that is distorted from the perovskite structure, and this distortion is attributed to the coexistence of two valence states, Bi^{3+} ($6s^2$) and Bi^{5+} ($6s^0$), due to charge disproportion of the formal Bi^{4+}. Octahedral BiO_6 breathes out and in for Bi^{3+} and Bi^{5+}, respectively[10]. Under hole-doping conditions, such as in $Ba_{1-x}K_xBiO_3$ ($x \sim 0.4$; ref. 5) and $BaBi_{1-x}Pb_xO_3$ ($x \sim 0.3$; refs 4,11), the breathing distortion is suppressed, resulting in a simple perovskite lattice[12] in which superconductivity emerges. Recent *ab initio* calculations[13] have assigned the higher T_c superconductivity to a correlation-enhanced electron–phonon coupling mechanism, stimulating the prediction and synthesis of new superconductor candidates among mixed-valent thallium perovskites[14–16]. The existing superconductivity has meant that research has mainly focused on hole-doped compounds, leaving electron-doped compounds relatively unexplored. In addition, the spin–orbit coupling (SOC) effect was not taken into account in previous theoretical study (ref. 13 and references therein), because the electronic states in the superconducting (hole-doped) region mainly result from Bi-6*s* and O-2*p* orbitals whose SOC effect is usually negligible.

By including the SOC effect in density-functional theory (DFT) calculations of the BBO band structure, we discovered a band inversion between the first (Bi-6*s* state) and second (Bi-6*p* state) conduction bands, which is stable against lattice distortions. This inversion indicates that BBO is a three-dimensional topological insulator with a large indirect energy gap of 0.7 eV when doped by electrons instead of holes. The band structure of ideal cubic BBO reveals that the conduction bands are modified markedly when SOC is included owing to the presence of the Bi-6*p* states, as illustrated in Fig. 1a. The first conduction band crossing the Fermi energy (E_F) has a considerable Bi-6*s* contribution over the whole Brillouin zone, except at the *R* momentum point where the Bi-6*p* contribution is dominant with the Bi-6*s* lying above it. Although one can see an inversion between Bi-6*p* and 6*s* states here, there is a zero energy gap at *R* without SOC because of the degeneracy of the *p* states. In previous literature that did not employ SOC, actually, this feature was already revealed. When SOC is included, we found that the $|p, j = 3/2\rangle$ and $|p, j = 1/2\rangle$ states split, which results in the large indirect energy gap of 0.7 eV in the vicinity of the *R* point. We point out that the band inversion strength is as large as nearly 2 eV, which is the energy difference between Bi-6*s* and $|p, j = 1/2\rangle$ states at the *R* point, as shown in Fig. 1b. Unlike bulk HgTe (ref. 17), a well-known topological insulator, this inversion occurs between the $|s, j = 1/2\rangle$ state and the $|p, j = 1/2\rangle$ state, rather than the $|p, j = 3/2\rangle$ state. As the Bi atom is the inversion centre of the perovskite lattice, the Bi-6*s* and Bi-6*p* states have + and − parities, respectively. Thus, a topological insulator state can be obtained if E_F is shifted up into this energy gap. The parities of all the valence bands below this gap were also calculated at all time-reversal invariant momenta, Γ, X, M and R, which yielded Z_2 topological invariants (1;111), confirming the topological non-trivial feature according to the parity criteria[18]. This is also consistent with a previous study of a topological insulator phase with Z_2 (1;111) in the perovskite lattice based on the model Hamiltonian[19]. At a doping rate of one electron per formula unit, E_F shifts inside the *s*–*p* inversion gap, and all the Bi ions become Bi^{3+}. Consequently, a cubic phase appears when the BiO_6 breathing distortion is suppressed, similar to the hole-doping case[12]. When the lone-pair Bi-6*s* state is fully occupied, we found that the new cubic lattice expands slightly in comparison with the undoped lattice. Although the *s* band becomes narrower in this case, the band inversion remains owing to the large *s*–*p* inversion strength (see Supplementary Fig. S1).

To illustrate the TSSs, we calculated the surface band structure using a slab model based on the Wannier functions extracted from the electron-doped bulk band structures. As an example, we take the surface to be oriented along the (001) direction on which the bulk *R* point is projected onto the $\bar{M}$ point (0.5,0.5,0) of the surface Brillouin zone. The slab is 30 BBO units thick with the outermost atomic layers being Ba–O. The TSSs, shown in Fig. 1c, exhibit a simple Dirac-cone-like energy dispersion. The Dirac cone exhibits square warping at higher energies due to the cubic symmetry of the lattice. The Fermi surface below the Dirac point exhibits a right-hand helical spin-texture on the top surface, similar to that of Bi_2Se_3-type topological insulator materials[20]. The spin polarization orients dominantly inside the surface plane with negligible out-of-plane components. The Fermi velocity near the Dirac point is

[1]Max Planck Institute for Chemical Physics of Solids, 01187 Dresden, Germany, [2]Max Planck Institute for the Physics of Complex Systems, 01187 Dresden, Germany, [3]Institute for Inorganic and Analytical Chemistry, Johannes Gutenberg University of Mainz, 55099 Mainz, Germany. *e-mail: yan@cpfs.mpg.de

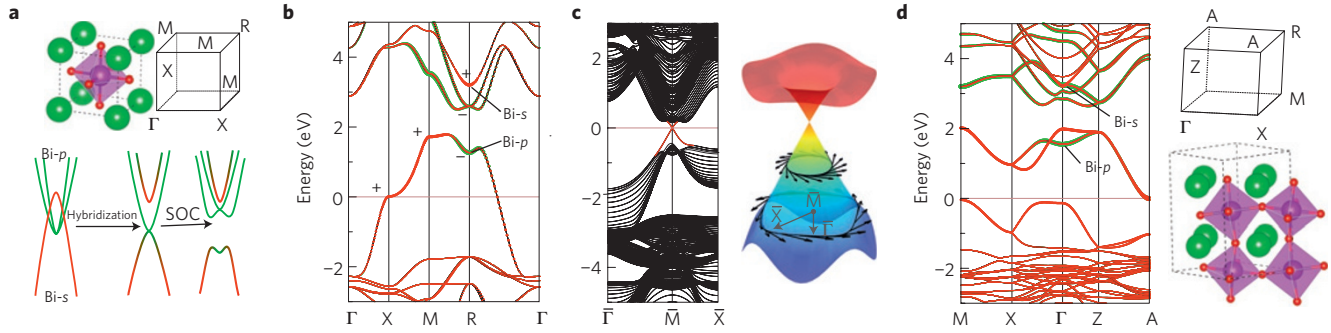

Figure 1 | Crystal structures and band structures of BBO. a, Ideal cubic perovskite lattice with the cubic Brillouin zone, and the band inversion process. The Bi atom is represented by the purple ball, O atoms by red balls and Ba atoms by green balls. Without SOC the Bi-*s* and Bi-*p* states are already inverted, resulting in two degenerate Bi-*p* bands at the R point. Subsequently, SOC splits this degeneracy and opens a large energy gap. **b**, Bulk band structure of the cubic lattice. The dispersions are shown along high-symmetry lines Γ(0 0 0)–X(0.5 0 0)–M(0.5 0.5 0)–R(0.5 0.5 0.5)–Γ, as labelled in the cubic Brillouin zone at the top of **a**. The Fermi energy is shifted to zero. The red and green dots indicate the Bi-*s* and Bi-*p* states, respectively, and corresponding parities are labelled. **c**, Surface band structure of an electron-doped BBO. The surface normal is along the (001) direction. Dispersions are along $\bar{\Gamma}$ (0 0)–$\bar{M}$ (0.5 0.5)–$\bar{X}$ (0.5 0) in the surface Brillouin zone. The red lines highlight the topological surface states inside the bulk bandgap. On the right of **c** is the three-dimensional plot of the surface Dirac cone near the $\bar{M}$ point with helical spin textures. **d**, Bulk band structure and lattice structure of the monoclinic $BiBaO_3$. The original R point of a cubic Brillouin zone in **a** is projected to the Γ point of the monoclinic Brillouin zone in **d**. Thus the band inversion exists at the Γ point in the monoclinic band structure, where Bi-*s* and Bi-*p* states are indicated. The effect of SOC is included in band structures **b**–**d**.

estimated to be approximately 0.75×10^5 m s^{-1}, and inside the large bulk energy gap, the TSSs are well localized on the surface atomic layers to about two BBO units or around 1 nm in thickness. On the other hand, to obtain the minimal effective model of the band topology, we derive a four-band Hamiltonian similar to that for Bi_2Se_3(ref. 6) in the basis of $|p;j=1/2,m_j=+1/2\rangle$, $|s;j=1/2,m_j=+1/2\rangle$, $|p;j=1/2,m_j=-1/2\rangle$, and $|s;j=1/2,m_j=-1/2\rangle$:

$$H(\mathbf{k})=\epsilon_0(\mathbf{k})\mathbb{I}_{4\times4}+\begin{pmatrix}\mathcal{M}(\mathbf{k}) & Ak_z & 0 & Ak_- \\ Ak_z & -\mathcal{M}(\mathbf{k}) & Ak_- & 0 \\ 0 & Ak_+ & \mathcal{M}(\mathbf{k}) & -Ak_z \\ Ak_+ & 0 & -Ak_z & -\mathcal{M}(\mathbf{k})\end{pmatrix} \quad (1)$$

where $\mathbf{k}=\mathbf{k}_0-\mathbf{k}_R$ (0.5, 0.5, 0.5) is centred at the R point, and $k_\pm=k_x\pm ik_y$, $\epsilon_0(\mathbf{k})=C+Dk^2$ and $\mathcal{M}(\mathbf{k})=M-Bk^2$. The main difference from that of the Bi_2Se_3 Hamiltonian is that equation (1) is isotropic to $\mathbf{k}$ owing to the cubic symmetry. We obtain the parameters of equation (1) by fitting the energy spectrum of the effective Hamiltonian to that of the *ab initio* calculations for the electron-doped cubic BBO using $M=-0.625$ eV, $A=2.5$ eV Å, $B=-9.0$ eV Å^2 and $D=1.5$ eV Å^2. Subsequently, the Fermi velocity of the TSSs is given by $v=A/\hbar\simeq0.5\times10^5$ m s^{-1}, which is consistent with the *ab initio* calculations.

We can confirm that the topological insulator phase is stable against lattice distortions. The monoclinic phase of BBO, as shown in Fig. 1d, is related to the O-breathing and -tilting distortions. In the monoclinic Brillouin zone, the original R point of a cubic lattice is projected to the Γ point owing to band folding. One can see that the *s*–*p* band inversion at this Γ point is still present and the indirect gap is unchanged (0.7 eV) in the bulk band structure. In addition, traditional *ab initio* DFT calculations may overestimate the band inversion owing to the underestimation of the bandgap. Therefore, we performed band structure calculations using the hybrid functional method[21], which is known to treat the dynamical correlation effect well for BBO (ref. 22). Here, we further validated the existence of band inversion for pristine cubic, electron-doped cubic and monoclinic distorted structures. (Details are described in the Supplementary Information.)

Experimentally, electron-doped BBO may be achieved in $BaBi(O_{0.67}F_{0.33})_3$ by substituting F for O atoms. The O and F atom have comparable atomic radii and electronegativities, which

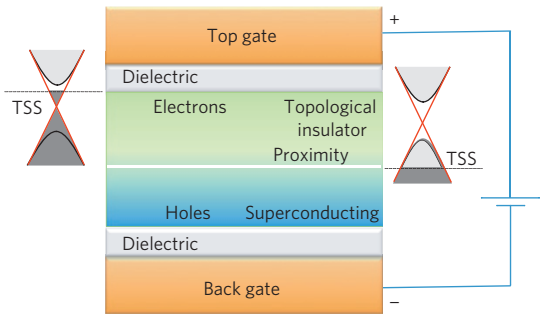

Figure 2 | Schematic of the interface between the topological insulator and superconducting state in a double-gated thin-film device. The top and bottom surfaces are the topological insulator and superconducting regions, respectively. The position of the Fermi energy (dashed lines) shifts down from the top to bottom surfaces in the band structure. In the middle region, TSSs are interfaced with superconducting states and become superconducting owing to the proximity effect.

can keep the octahedral BiO_6 stable. For example, F substitution for O was applied for the iron-based superconductor LaOFeAs to realize electron doping[23]. It is also possible to employ a state-of-the-art electrolyte gating technique to BBO to induce heavy electron doping, which has been realized for several mixed-valent compounds such as ZrNCl (ref. 24) and VO_2 (ref. 25). In particular, the electrolyte gating of VO_2 leads to the creation of oxygen vacancies, which induce a stable metallic phase even when removing the electrolyte[25]. As for the VO_2 case, we expect that electrolyte gating can also reach large electron doping by generating considerable oxygen vacancies, which were commonly observed as electron donors for BBO in previous experiments[26]. On the other hand, although the TSSs are unoccupied in pristine BBO compounds, it may be possible to monitor these states directly through monochromatic two-photon photoemission, as was recently employed to monitor the empty TSSs of Bi chalcogenides[27].

Thus far we can state that BBO becomes a superconductor with hole doping and a potential topological insulator with electron doping. If pn-junction-type devices are fabricated with BBO, an interface between the TSSs and the superconductor may be realized, which is necessary for the realization of the Majorana fermion proposal[9] for quantum computation. Here, we

outline a double-gated thin-film configuration, as illustrated in Fig. 2. If the bottom and top regions of the film are predoped as p and n type, respectively, the double-gated structure may feasibly induce a hole-rich bottom surface and an electron-rich top surface, resulting in TSSs and superconductivity states on the top and bottom surfaces, respectively. In the middle region of the slab, the TSSs overlap with the bulk bands and penetrate the bulk. These TSSs can then become superconducting as a result of the proximity effect with the bottom superconducting regime. Such a structure is likely to be attainable as high-quality BBO thin films, which have been successfully grown on $SrTiO_3$ (refs 28–30) and MgO (ref. 30) substrates. Moreover, the O-tilting lattice distortion was recently found to be suppressed in a BBO(001) thin film on MgO (ref. 30), which is very close to our required cubic structure.

The band structure of $BaBiO_3$ can act as a prototype for designing new perovskite topological insulators. Sc, Y or La can be substituted for Ba to obtain new compounds as analogues of an electron-doped BBO. We found in calculations that a similar band inversion exists in this case. However, these compounds are semimetals (the Sc/Y/La-*d* orbitals are lower in energy than the Bi-*p* states) and induce topological semimetals (see Supplementary Information). In contrast, $CsTlCl_3$-type halide perovskites, which are predicted to be superconductor candidates[14–16], have band structures that are similar to BBO. However, we did not observe *s*–*p* inversion for $ATlX_3$ (A = Cs, Rb, X = F, Cl, Br, I), because the SOC of Tl is not strong enough. When we can substitute Sn or Pb for Tl, we find that heavier members of this family, such as $CsPbI_3$, are near the boundary of a topological trivial–non-trivial phase transition. Compressive pressure is necessary to drive these boundary materials into the topological insulator region, which is consistent with recent theoretical calculations of these halides[31].

Methods

In band structure calculations, we employed *ab initio* DFT with the generalized gradient approximation. We employed the Vienna *ab initio* simulation package with a plane wave basis[32]. The core electrons were represented by the projector-augmented-wave potential. For hybrid-functional calculations, we adopted the HSE06 (ref. 21) type of functionals and interpolated the band structures using Wannier functions[33], where the DFT wavefunctions were projected to Bi-*sp*, Ba-*d* and O-*p* orbitals. We adopted the lattice constants from their experimental values for both the cubic[34] ($a = 4.35$ Å) and monoclinic structures[10].

Received 8 April 2013; accepted 15 August 2013; published online 22 September 2013

References

1. Qi, X-L. & Zhang, S-C. Topological insulators and superconductors. *Rev. Mod. Phys.* **83,** 1057–1110 (2011).
2. Hasan, M. Z. & Kane, C. L. Colloquium: Topological insulators. *Rev. Mod. Phys.* **82,** 3045–3067 (2010).
3. Yan, B. & Zhang, S-C. Topological materials. *Rep. Prog. Phys.* **75,** 096501 (2012).
4. Sleight, A. W., Gillson, J. L. & Bierstedt, P. E. High-temperature superconductivity in the $BaPb_{1-x}Bi_xO_3$ systems. *Solid State Commun.* **17,** 27–28 (1975).
5. Cava, R. J. *et al.* Superconductivity near 30 K without copper: The $Ba_{0.6}K_{0.4}BiO_3$ perovskite. *Nature* **332,** 814–816 (1988).
6. Zhang, H. *et al.* Topological insulators in Bi_2Se_3, Bi_2Te_3 and Sb_2Te_3 with a single Dirac cone on the surface. *Nature Phys.* **5,** 438–442 (2009).
7. Xia, Y. *et al.* Observation of a large-gap topological-insulator class with a single Dirac cone on the surface. *Nature Phys.* **5,** 398–402 (2009).
8. Chen, Y. L. *et al.* Experimental realization of a three-dimensional topological insulator, Bi_2Te_3. *Science* **325,** 178–181 (2009).
9. Fu, L. & Kane, C. L. Superconducting proximity effect and Majorana fermions at the surface of a topological insulator. *Phys. Rev. Lett.* **100,** 096407 (2008).
10. Cox, D. E. & Sleight, A. W. Crystal structure of $Ba_2Bi_{3+}Bi_{5+}O_6$. *Solid State Commun.* **19,** 969–973 (1976).
11. Khan, Y., Nahm, K., Rosenberg, M. & Willner, H. Superconductivity and semiconductor–metal phase transition in the system $BaPb_{1-x}Bi_xO_3$. *Phys. Status Solidi A* **39,** 79–88 (1977).
12. Pei, S. *et al.* Structural phase diagram of the $Ba_{1-x}K_xBiO_3$ system. *Phys. Rev. B* **41,** 4126–4141 (1990).
13. Yin, Z. P., Kutepov, A. & Kotliar, G. Correlation-enhanced electron–phonon coupling: Applications of *GW* and screened hybrid functional to bismuthates, chloronitrides, and other high-T_c superconductors. *Phys. Rev. X* **3,** 021011 (2013).
14. Yin, Z. P. & Kotliar, G. Rational material design of mixed-valent high-Tc superconductors. *Europhys. Lett.* **101,** 27002 (2013).
15. Retuerto, M. *et al.* Synthesis and properties of the theoretically predicted mixed-valent perovskite superconductors: $CsTlX_3$ (X = F, Cl). Preprint at http://arxiv.org/abs/1302.2353 (2013).
16. Schoop, L. M., Müchler, L., Felser, C. & Cava, R. J. Lone pair effect, structural distortions and potential for superconductivity in Tl perovskites. *Inorg. Chem.* **52,** 5479–5483 (2013).
17. Bernevig, B. A., Hughes, T. L. & Zhang, S. C. Quantum spin hall effect and topological phase transition in HgTe quantum wells. *Science* **314,** 1757–1761 (2006).
18. Fu, L. & Kane, C. L. Topological insulators with inversion symmetry. *Phys. Rev. B* **76,** 045302 (2007).
19. Weeks, C. & Franz, M. Topological insulators on the Lieb and perovskite lattices. *Phys. Rev. B* **82,** 085310 (2010).
20. Hsieh, D. *et al.* A tunable topological insulator in the spin helical Dirac transport regime. *Nature* **460,** 1101–1105 (2009).
21. Heyd, J., Scuseria, G. E. & Ernzerhof, M. Erratum: Hybrid functionals based on a screened Coulomb potential [J. Chem. Phys. 118, 8207 (2003)]. *J. Chem. Phys.* **124,** 219906–1 (2006).
22. Franchini, C., Sanna, A., Marsman, M. & Kresse, G. Structural, vibrational, and quasiparticle properties of the Peierls semiconductor $BaBiO_3$: A hybrid functional and self-consistent GW+vertex-corrections study. *Phys. Rev. B* **81,** 085213 (2010).
23. Kamihara, Y., Watanabe, T., Hirano, M. & Hosono, H. Iron-based layered superconductor $LaO_{1-x}F_xFeAs$ ($x = 0.05$–0.12) with $T_c = 26$ K. *J. Am. Chem. Soc.* **130,** 3296–3297 (2008).
24. Ye, J. *et al.* Liquid-gated interface superconductivity on an atomically flat film. *Nature Mater.* **9,** 125–128 (2009).
25. Jeong, J. *et al.* Suppression of metal-insulator transition in Vo_2 by electric field–induced oxygen vacancy formation. *Science* **339,** 1402–1405 (2013).
26. Suzuki, M. & Murakami, T. Effect of oxygen vacancies on carrier localization in $BaPb_{1-x}Bi_xO_3$. *Solid State Commun.* **53,** 691–694 (1985).
27. Niesner, D. *et al.* Unoccupied topological states on bismuth chalcogenides. *Phys. Rev. B* **86** (2012).
28. Sato, H., Tajima, S., Takagi, H. & Uchida, S. Optical study of the metal-insulator transition on $Ba_{1-x}K_xBi0_3$ thin films. *Nature* **338,** 241–243 (1989).
29. Gozar, A., Logvenov, G., Butko, V. & Bozovic, I. Surface structure analysis of atomically smooth $BaBiO_3$ Films. *Phys. Rev. B* **75,** 201402 (2007).
30. Inumaru, K., Miyata, H. & Yamanaka, S. Partial suppression of structural distortion in epitaxially grown $BaBiO_3$ thin films. *Phys. Rev. B* **78,** 132507 (2008).
31. Jin, H., Im, J. & Freeman, A. J. Topological insulator phase in halide perovskite structures. *Phys. Rev. B* **86,** 121102 (2012).
32. Kresse, G. & Hafner, J. Ab initio molecular dynamics for liquid metals. *Phys. Rev. B* **47,** 558–561 (1993).
33. Mostofi, A. A. *et al.* Wannier90: A tool for obtaining maximally-localised Wannier functions. *Comput. Phys. Commun.* **178,** 685–699 (2008).
34. Cox, D. E. & Sleight, A. W. Mixed-valent $Ba_2Bi_{3+}Bi_{5+}O_6$: Structure and properties vs temperature. *Acta Crystallogr. B* **35,** 1–10 (1979).

Acknowledgements

We thank X-L. Qi and S-C. Zhang, S. S. P. Parkin, Y-L. Chen, Z. Wang and J. Kuebler for fruitful discussions. B.Y. acknowledges financial support from the ERC Advanced Grant (291472) and computing time at HLRN Berlin/Hannover (Germany).

Author contributions

B.Y. and C.F. conceived the project on oxide topological insulators. B.Y. proposed the oxide material and the superconductor/topological insulator interface, performed calculations and wrote the paper. M.J. analysed lattice distortions and electron doping. C.F. supervised the project.

Additional information

Supplementary information is available in the online version of the paper. Reprints and permissions information is available online at www.nature.com/reprints. Correspondence and requests for materials should be addressed to B.Y.

Competing financial interests

The authors declare no competing financial interests.